Composite Structures 340 (2024) 118170

Contents lists available at ScienceDirect

Composite Structures

journal homepage: www.elsevier.com/locate/compstruct

Analysis of raw-crushed wind-turbine blade as an overall concrete addition: Stress–strain and deflection performance effects

Vanesa Ortega-López [a,b], Flora Faleschini [b], Nerea Hurtado-Alonso [c], Javier Manso-Morato [a], Víctor Revilla-Cuesta [a,b,*]

[a] Department of Civil Engineering, Escuela Politécnica Superior, University of Burgos, c/ Villadiego s/n, 09001 Burgos, Spain
[b] Department of Civil, Environmental and Architectural Engineering, University of Padova, via Francesco Marzolo 9, 35131 Padova, Italy
[c] Department of Construction, Escuela Politécnica Superior, University of Burgos, c/ Villadiego s/n, 09001 Burgos, Spain

ARTICLE INFO

Keywords:
Raw-crushed wind-turbine blade
Concrete
Stress-strain curve
Transverse deformation
Load-deflection curve
Deformability under indirect-tensile stresses

ABSTRACT

End-of-life wind-turbine blades undergo non-selective crushing to produce Raw-Crushed Wind-Turbine Blade (RCWTB), which can be recycled as a raw material in concrete. RCWTB contains fibers from glass fiber-reinforced polymer that can add ductility and load-bearing capacity to concrete. Concrete mixes with percentage additions of between 0.0 % and 6.0 % RCWTB by volume are produced to analyze their compressive stress–strain performance, their deflection under bending forces, and their deformability under indirect-tensile stresses. Higher RCWTB contents increased deformability in the longitudinal direction under compression, the concrete material absorbing energy levels that were up to 111.4 % higher, even though additions of only 6.0 % RCWTB were sufficient to strengthen the load-bearing capacity. RCWTB fiber stitching effect was most noticeable in the transverse direction under compression, as it reduced elastic deformability and failure strain, removed the yield step caused by vertical-splitting cracking, and increased the fracture strain by up to 94.4 %. With regard to deflection, RCWTB fibers conditioned concrete compliance at advanced ages without any dependence on the modulus of elasticity, and percentage additions from 3.0 % provided load-bearing capacity. This advantage was also noted in indirect-tensile stresses for 6.0 % RCWTB. In summary, RCWTB successfully increased the ductility and load-bearing capacity of concrete *per* unit strength and carbon footprint.

1. Introduction

Concrete is the most widely used structural material in the civil-engineering sector [1]. Its main characteristic is its strength behavior, and its key property is compressive strength [2]. However, if the in-service behavior of a concrete component is to be accurately predicted and sudden failure avoided [3], then knowledge of its deformational behavior is also necessary at the design stage [4]. Deformational behavior has to be evaluated especially under compressive and bending stresses, the most common stresses to which a concrete components are subjected [5,6]. Examples of the deformational behavior of concrete samples taken from studies of the authors published elsewhere [7,8] are shown below in Fig. 1.

The deformational behavior in a longitudinal direction (*i.e.,* parallel to the load) of some concrete specimens under compressive stress is reflected by the stress–strain curves on the center of Fig. 1. Those curves are characterized in their initially linear sections that reflect some proportionality between stress and strain [9]. The proportionality constant is the modulus of elasticity, with values of around 30 GPa [10]. At approximately 50–60 % of its failure stress (compressive strength), any proportionality between stress and strain is lost, and a zone of plastic behavior begins and ends at failure [7]. Strain levels are low in the longitudinal direction, with failure strain estimated at 2000 μm/m and a strain at fracture of around 3000–3500 μm/m according to different international standards [11,12].

The stress–strain curve in the transverse direction to compressive loading (Fig. 1 left) was similar to the same curve obtained in the longitudinal direction, although there were two major differences. On the one hand, the yield step or transition between the elastic- and plastic-behavior zones, in which strain increased without any variation in stress [13]. The yield step coincided with the appearance of micro-cracking, due to vertical splitting that propagated towards the axis of the concrete specimen under compression [7]. On the other hand, the elastic strain in the transverse direction was much lower than in the

* Corresponding author at: Department of Civil Engineering, Escuela Politécnica Superior, University of Burgos, c/ Villadiego s/n, 09001 Burgos, Spain.
E-mail address: vrevilla@ubu.es (V. Revilla-Cuesta).

https://doi.org/10.1016/j.compstruct.2024.118170
Received 11 January 2024; Received in revised form 1 April 2024; Accepted 3 May 2024
Available online 4 May 2024

longitudinal direction [14]. These are generally estimated to be 5 times less, hence the Poisson's coefficient of 0.2 units usually considered for concrete [11,12]. However, strain was amplified in the zone of plastic behavior, especially when the applied stress approached the ultimate compressive strength, until it was around 2 or 3 times greater than the longitudinal strain [15]. It is usual to consider 7000–8000 μm/m as transverse strain at fracture [11,12].

Finally, in terms of bending performance (Fig. 1 right), the load–deflection curve of the concrete specimens initially showed a curved zone characterized by the onset of micro-cracking, due to slight yielding of in this case the concrete specimen under loading [16]. The curved zone was then followed by a more linear zone where the inverse of the slope, also referred to as the compliance of the specimen, showed its bending stiffness, *i.e.*, the extent to which the concrete specimen could withstand deflection [17]. This proportionality between load and deflection is usually maintained until failure [8].

In any of the three situations mentioned above, as the applied load was increased, cracks continued to appear in the concrete specimens up until failure. Brittle concrete failure occurred, without prior warning except for the appearance of the aforementioned cracking [18]. The addition of fibers modifies the deformational behavior of the concrete in two ways. First, the fibers stitch the cementitious matrix, which decreases cracking when the concrete is loaded, thus increasing concrete deformability [1]. The stitching effect even delays the yield step due to vertical micro-cracking in the transverse direction to compressive loading [13]. Secondly, the fibers ensure that no sudden failure can take place, but that the concrete component is still capable of supporting some load after failure while increasing its strain levels [19]. This effect, known as load-bearing capacity, is especially noticeable. It is crucial in concrete components undergoing bending [20], as it ensures, sufficient time for the evacuation of a structure that might otherwise undergo sudden failure [21].

Those effects are most notably demonstrated by metallic fibers, due to their high modulus of elasticity [22]. In bending behavior, they can even mean that a concrete component can support higher post-failure loads than the failure load [13]. Other fiber types, such as synthetic fibers, also contribute to those aspects, although to a lesser extent, due to their greater deformability [23,24]. The same advantages are also evident in the use of recycled fibers when added in the right proportions [25,26]. Adding a very low content can render the above-mentioned effects almost imperceptible, while they can be counterproductive in very high quantities, mainly in terms of strength [27]. The specific characteristics of each recycled fiber means that a separate analysis is needed of the effect of each fiber type on deformational behavior [28,29].

Work began in the wind-energy sector on the dismantlement of the first wind farms and the consequent recycling of the wind turbines that had reached the end of their service life in the present decade [30]. Recovery and recycling of wind-turbine blades are complicated processes, due to their composition based on Glass Fiber-Reinforced Polymer (GFRP) composite, polyurethane, and balsa wood [31]. Solutions have therefore been sought ranging from the reconditioning of the blades as urban furniture [31] to their chemical treatment [32], mainly either pyrolysis or solvolysis, to separate out their components for alternative uses [33]. Once separated, GFRP composites have also been used as powder or aggregate in the manufacture of concrete, although the results have not been encouraging [34,35]. However, initial attempts to cut slender GFRP-composite elements, which are then added to the concrete as fibers that can effectively stitch the cementitious matrix, have been shown to reduce concrete deformability and strengthen load-bearing capacity in the same way as conventional fibers [35]. In another investigation, the feasibility of using GFRP-composite fibers produced by blade crushing was evaluated [36], yielding comparable effects to the fibers produced by the cut of slender GFRP elements. However, the main approach has been to add only GFRP-composite fibers to concrete, which implies that the GFRP composite has to be separated from the other blade components, *i.e.*, balsa wood and polyurethane, prior to chemical treatment or mechanical cutting, or after crushing and sieving the entire blade [37]. These additional post-crushing processes make the blade recovery processes more expensive and add to their carbon footprint.

The aim of this study is to analyze the deformational behavior of concrete produced with Raw-Crushed Wind-Turbine Blade (RCWTB), a waste material obtained from the non-selective crushing of wind-turbine blades, *i.e.*, with no separation of components [38]. RCWTB therefore consists of GFRP-composite fibers mixed up with approximately spherical particles of balsa wood and polyurethane [38]. Five concrete mixtures were prepared with percentage additions of between 0.0 % and 6.0 % RCWTB by volume, which were tested in compression, bending and indirect-tensile tests, continuously recording loads/stresses and deflections/strains. In that way, longitudinal and transverse stress–-strain curves under compression, load–deflection curves under bending, and deformational curves under indirect-tensile stresses were obtained. The final objective was to define what RCWTB content is necessary to effectively increase the ductility of concrete. To the best of the authors' knowledge, those aspects related to the deformational behavior of concrete produced with this type of waste have not been analyzed in any other study on the recovery of wind-turbine blades as raw materials for concrete production.

2. Materials and methods

2.1. Concrete components

In addition to mains water, the concrete mixes were prepared with locally sourced raw materials. First, CEM II/A-L 42.5 R as *per* EN 197-1 [39], an ordinary Portland cement with small additions of limestone. Second, crushed siliceous aggregate, supplied in 0/2 mm, 2/6 mm, and

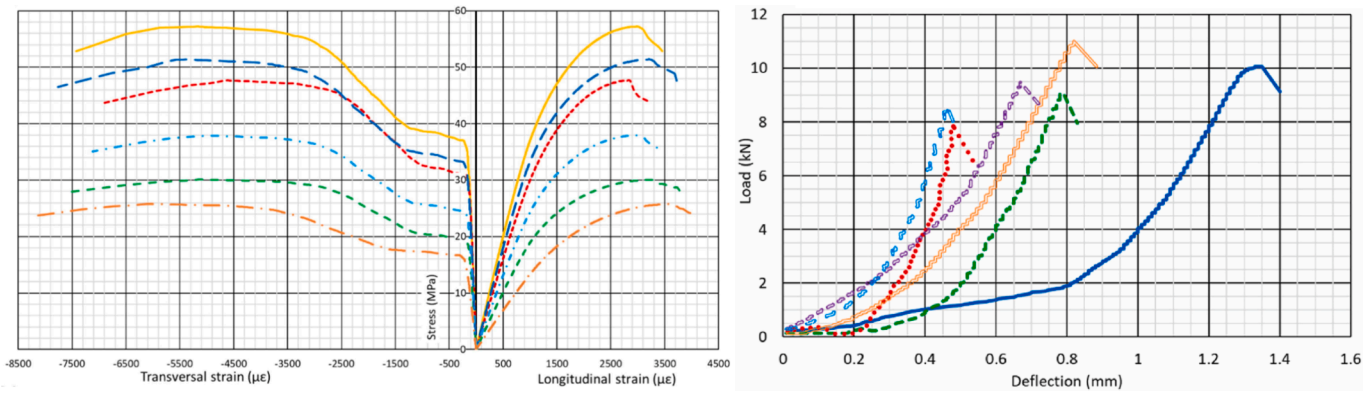

Fig. 1. Examples of longitudinal and transverse stress–strain curves under compression (left) [7] and load–deflection curves under bending (right) [8].

Table 1
Physical properties of crushed siliceous aggregate.

Aggregate fraction	Saturated-surface-dry density (kg/dm^3)	24-hour water absorption (% wt.)
0/2 mm	2.62	0.52
2/6 mm	2.58	1.83
6/22 mm	2.59	1.66

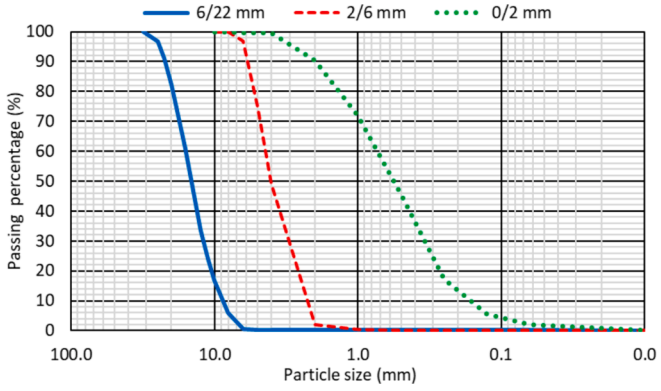

Fig. 2. Gradation curves of crushed siliceous aggregate.

6/22 mm fractions, whose physical properties and gradation curves are shown in Table 1 and Fig. 2, respectively. Finally, two plasticizers, which improved concrete workability without increasing the water content.

The RCWTB was obtained in two phases. The first phase consisted of crushing pieces from the central part of wind-turbine blades (LM21 model), which basically comprised sandwich panels of GFRP, balsa wood, and polyurethane. Crushing took place in a knife mill, identical to the ones used to crush plastic [40], that ground up the different components to obtain GFRP-composite fibers, composite micro-fibers agglomerated in the form of "fluffs", and approximately spherical particles of balsa wood and polyurethane. In the second phase, sieving ensured that all the components could pass through a 10-mm-aperture sieve. This sieve size was defined experimentally and allowed ensuring adequate sizes of GFRP-composite fibers and balsa-wood and polyurethane particles for concrete production to maximize the stitching effect of the GFRP-composite fibers. Those components that could not pass through the sieve were once again subjected to cyclical crushing and sieving. RCWTB had a density of 1.63 kg/dm^3 according to EN 1097-6 [39], and its composition was 66.8 % by weight of GFRP-composite fibers, 6.3 % by weight of balsa-wood particles, 8.3 % by weight of polyurethane particles, and 18.6 % by weight of composite micro-fibers. The GFRP-composite fibers had an average length in the longitudinal direction of 13.1 mm and an equivalent diameter of 0.73 mm. The particles of balsa wood and polyurethane had a size mainly between 2 and 5 mm. A photograph of the material is shown in Fig. 3. Further details of this RCWTB can be found in a previous paper of the authors [38].

Fig. 3. Raw-crushed wind-turbine blade.

2.2. Mix design

The mix was designed to analyze the performance of concrete with percentage additions between 0.0 % and 6.0 % RCWTB by volume. Thus, the fiber additions achieved were similar to the amounts described in another study of the authors on fiber-reinforced concrete [13]. RCWTB was added as an overall addition, so that the cement content *per* m^3 of concrete decreased. In doing so, the RCWTB fibers added some strength, partially compensating for the decrease in cement content, which in turn reduced the overall carbon footprint of the concrete, to which cement is by far the largest contributor [41].

First, the *M0.0* reference mix was designed. To do so, the content of each aggregate fraction was defined by calculating the optimal particle packing ratios according to the Fuller's curve. Thus, the 0/2 mm fraction represented 24.8 % of the total aggregate volume; the 2/6 mm fraction, 30.1 %; and the 6/22 mm fraction, 45.1 %. In addition, a conventional cement content (320 kg/m^3), a water/cement ratio of 0.40, and a combined content of both plasticizers of 1.0 % of the cement mass were selected. It resulted in an S3 slump class (slump of 12.5 ± 2.5 mm) concrete as *per* EN 206 [39] of adequate strength for structural use. Based on the composition of the *M0.0* mix, percentage additions of 1.5 %, 3.0 %, 4.5 %, and 6.0 % RCWTB by volume were added, to produce the mixes *M1.5*, *M3.0*, *M4.5*, and *M6.0*, respectively. The water and the plasticizer contents were increased when the residue was added, in order to preserve the slump class. In this way, workability had no effect on the results since similar compaction levels were reached in the vibration phase for all the concrete mixes. The RCWTB was always embedded in the concrete mass in similar conditions while the concrete mixes exhibited workability levels suitable for use [7]. The comparative compositions of all the mixes are shown in Table 2 and their adjustment to the S3 slump class (EN 206 [39]) is also specified in the last row.

Table 2
Comparative design of concrete mixes (kg) and slump.

Mix component	*M0.0*	*M1.5*	*M3.0*	*M4.5*	*M6.0*
Cement	320				
Aggregate (0/2 mm # 2/6 mm # 6/22 mm)	500 # 600 # 900				
Water	128	133	137	142	146
Plasticizer 1 # Plasticizer 2	2.20 # 1.10	2.62 # 1.31	3.04 # 1.52	3.46 # 1.73	3.88 # 1.94
RCWTB	0.0	24.5	49.0	73.5	98.0
Slump (cm)	10.0	10.5	13.0	13.5	12.0

RCWTB additions without modifying the amount of the other concrete components increased the produced volume and, therefore, reduced the cement content *per* cubic meter.

2.3. Experimental plan

After mixing, the slump of the mixes was tested in accordance with EN 12350-2 [39], the results of which are shown in Table 2. Subsequently, the specimens to be used in the hardened-state tests were prepared. The specimens were demolded 24 h after manufacture and stored in a humid chamber as *per* EN 12390-2 [39] until the testing ages. Each test was performed on three specimens and the arithmetic mean of all three results are presented in this paper.

Three different hardened-state tests were performed on each mix to evaluate the deformational behavior of concrete with RCWTB as an overall addition:

- 10 × 20-cm cylindrical specimens underwent deformational behavior tests under compression at 90 days. Compressive-strength tests were conducted as *per* EN 12390-3 [39], by applying compressive loading that was increased monotonically at a rate of 2kN/s until specimen breakage. However, unlike the conventional compressive-strength test, continuous measurements of both the load and the longitudinal and transverse strains were performed with a load cell and six strain gauges, respectively. Three strain gauges were placed in the longitudinal direction to the load and another three in the transverse direction. The longitudinal and the transverse stress–strain curves under compression could then be plotted with the recorded data for each mix and analyzed [9].
- Deflection-behavior tests were performed under bending at 7 and 90 days on 7.5 × 7.5 × 27.5-cm prismatic specimens. The test was identical to a four-point flexural-strength test as *per* EN 12390-5 [39], so the load was gradually increased until failure using a displacement control at a rate of 0.40 mm/min. Nevertheless, in order to evaluate the load-bearing capacity of the concrete, the test was not ended after the maximum load had been applied, but when the specimen was no longer able to support any load. The test press was set up for continuous recording of the applied load and the displacement of the load-application piston during the test, the results of which determined the load–deflection curves at both ages. The load–deflection curves were studied at 7 days (early age) and at 90 days (advanced age), for a detailed evaluation over time of the RCWTB fibers and their effect on the load-bearing capacity of the concrete specimens, an effect usually found under bending [19,21].
- Deformability tests on 10 × 20-cm cylindrical specimens under indirect-tensile stresses were performed at 90 days to evaluate the load-bearing capacity of the concrete, as with the deflection-behavior test. A Brazilian splitting test as *per* EN 12390-6 [39] was therefore conducted. Thus, the cylindrical specimen was supported on one of its generatrixes, while a continuously increasing load was applied on the opposite generatrix until the specimen was no longer able to support any load. The stress increment was set at 0.04 MPa/s, the minimum value in the above-mentioned standard, so optimum recording of the load that the press was applying and the displacement of the load-application piston was ensured [7]. The results of that test provided a representation of the deformational curves under indirect-tensile stresses (indirect-tensile strength vs. piston displacement).

Some mechanical properties of the concrete mixes of this study are presented elsewhere [42]. They are also introduced in this paper to analyze its relationship with the strain, deflection and absorbed-energy values.

3. Results and discussion

3.1. Longitudinal stress–strain performance under compression

The main results that can be drawn from the deformational-behavior test under compression in the longitudinal direction are detailed in Table 3. The longitudinal stress–strain curves are depicted in Fig. 4.

3.1.1. Performance analysis

The longitudinal stress–strain curves under compression revealed the elastic- and the plastic-behavior zones described in the introduction, as shown in Fig. 4. In that case, the higher the RCWTB content, the lower the modulus of elasticity. Moreover, the plastic-behavior zone also encompassed a wider range of strains with increasing RCWTB contents. The addition of RCWTB therefore increased both elastic and plastic deformability, *i.e.*, concrete ductility. The values provided in Table 3 clearly underline that performance.

In relation with the elastic-behavior zone, the modulus of elasticity decreased approximately linearly up to additions of 4.5 % RCWTB (Table 3). Fibers allow very slightly increasing the elastic stiffness of concrete by stitching the cementitious matrix if no other aspect of the concrete composition is modified when adding them [43]. In this case,

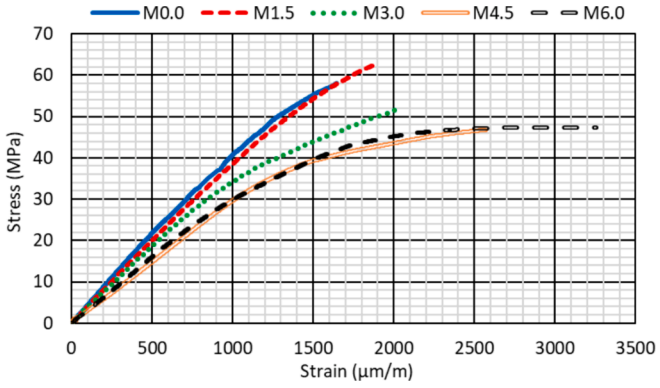

Fig. 4. Longitudinal stress–strain curves under compression.

Table 3
Key values of the longitudinal stress–strain behavior under compression.

Property	Parameters	*M0.0*	*M1.5*	*M3.0*	*M4.5*	*M6.0*
Modulus of elasticity	**Value (GPa)**	41.4	38.4	34.4	28.9	30.4
	Δ RCWTB content (%)	0.0	−7.4	−17.0	−30.1	−26.6
Strain at the limit of proportionality	**Value (μm/m)**	824	1013	985	1149	918
	Δ RCWTB content (%)	0.0	22.9	19.5	39.4	11.4
Compressive strength (failure stress)	**Value (MPa)**	58.0	62.8	52.2	46.8	47.4
	Δ RCWTB content (%)	0.0	8.3	−10.0	−19.3	−18.3
Failure strain	**Value (μm/m)**	1645	1892	2039	2571	2942
	Δ RCWTB content (%)	0.0	15.0	24.0	56.3	78.8
Strain at fracture	**Value (μm/m)**	1645	1892	2039	2571	3255
	Δ RCWTB content (%)	0.0	15.0	24.0	56.3	97.9
Absorbed energy	**Value (MJ/m^3)**	0.0536	0.0637	0.0662	0.0791	0.1133
	Δ RCWTB content (%)	0.0	18.8	23.5	47.6	111.4

'**Δ RCWTB content (%)**' refers to the percentage variation with respect to the *M0.0* reference mix.

the effect of the RCWTB fibers may have been that. However, the necessary increase in the water/cement ratio to preserve workability when adding RCWTB (Table 2) [13], and mainly the presence of polyurethane and balsa-wood particles in this waste, which are more flexible than natural-aggregate particles [44], may have also offset the stitching effect and reduced the elastic stiffness. This behavior was not reproduced with RCWTB additions of 6.0 %, as there were sufficiently large amounts of fibers within the concrete to compensate for both negative aspects. The decrease in the modulus of elasticity was not linked to an increase in the strain at the limit of proportionality, as might have been expected on the basis of other studies [7]. Although that strain level increased following the addition of RCWTB, no clear trend was found, as the increases in strain levels observed at the limit of proportionality were of 39.4 % and 11.4 %, respectively, between the *M0.0* and the *M4.5* mixes and between the *M0.0* and *M6.0* mixes.

The use of RCWTB also affected the levels of compressive strength (Table 3). The addition of 1.5 % RCWTB increased compressive strength levels by 8.3 % with respect to the *M0.0* mix as a result of the fiber crack-stitching effect, thus compensating for the weakening effects of increasing the water/cement ratio (Table 2) [45] and the presence of balsa-wood and polyurethane particles [46]. Then, the compressive strength followed similar trends with higher additions of RCWTB than the modulus of elasticity. Thus, it decreased in the *M3.0* and *M4.5* mixes (maximum decrease of 19.3 % in the *M4.5* mix), due to the two negative aspects described above. Similar performance for the compressive strength and the modulus of elasticity has also been obtained when adding other types of plastic fibers to concrete [47,48]. However, compressive strength was almost identical in the *M4.5* and *M6.0* mixes, at around 47 MPa, so additions of 6.0 % RCWTB may provide a sufficient fiber proportion within the concrete for the stitching effect to predominate [28].

Regardless of the strength behavior, the failure strain of concrete always increased following RCWTB additions (Table 3). In an initial approach, that effect can be intuitively attributed to two aspects. On the one hand, the first aspect was the greater flexibility of polyurethane and balsa-wood particles compared to the crushed siliceous aggregate that they replaced [44]. Nevertheless, it was thought to have had little influence, because those particles could also favor cracking at high loads, due to a weaker interfacial transition zones than those of natural aggregate [49], thereby mainly influencing the elastic behavior of the samples. On the other hand, the second aspect was the fiber stitching effect that limited concrete cracking [18]. That effect is also the generally intended purpose of commercial fibers, so that a concrete structure will show early warning signs of possible collapse, withstanding higher strain levels and avoiding sudden brittle failure [16]. Under compressive stress, the fibers present in the RCWTB effectively strengthened the concrete specimens: the higher the percentage additions of RCWTB, the more noticeable the strengthening effect. Thus, the failure strain was 78.8 % higher in the *M6.0* mix than in the *M0.0* mix (2942 μm/m vs. 1645 μm/m).

The fracture-strain values also reflected increased deformability in the plastic region (Table 3). Failure strain and fracture strain coincided up to RCWTB contents of 4.5 %. However, the fracture strain of the *M6.0* mix was around 300 μm/m higher than the failure strain. Those results clearly reflected that the RCWTB-fiber stitching effect added load-bearing capacity under compression, *i.e.*, the concrete was still capable of withstanding load after breakage at higher strain levels [16]. The RCWTB fiber-stitching effect under compression was therefore comparable to commercial fibers [13,20]. The increased deformability following the addition of RCWTB was also evident from the increase in absorbed energy (Table 3) of the *M6.0* mix, which was twice that of the *M0.0* mix. RCWTB clearly helped to increase concrete ductility, as was

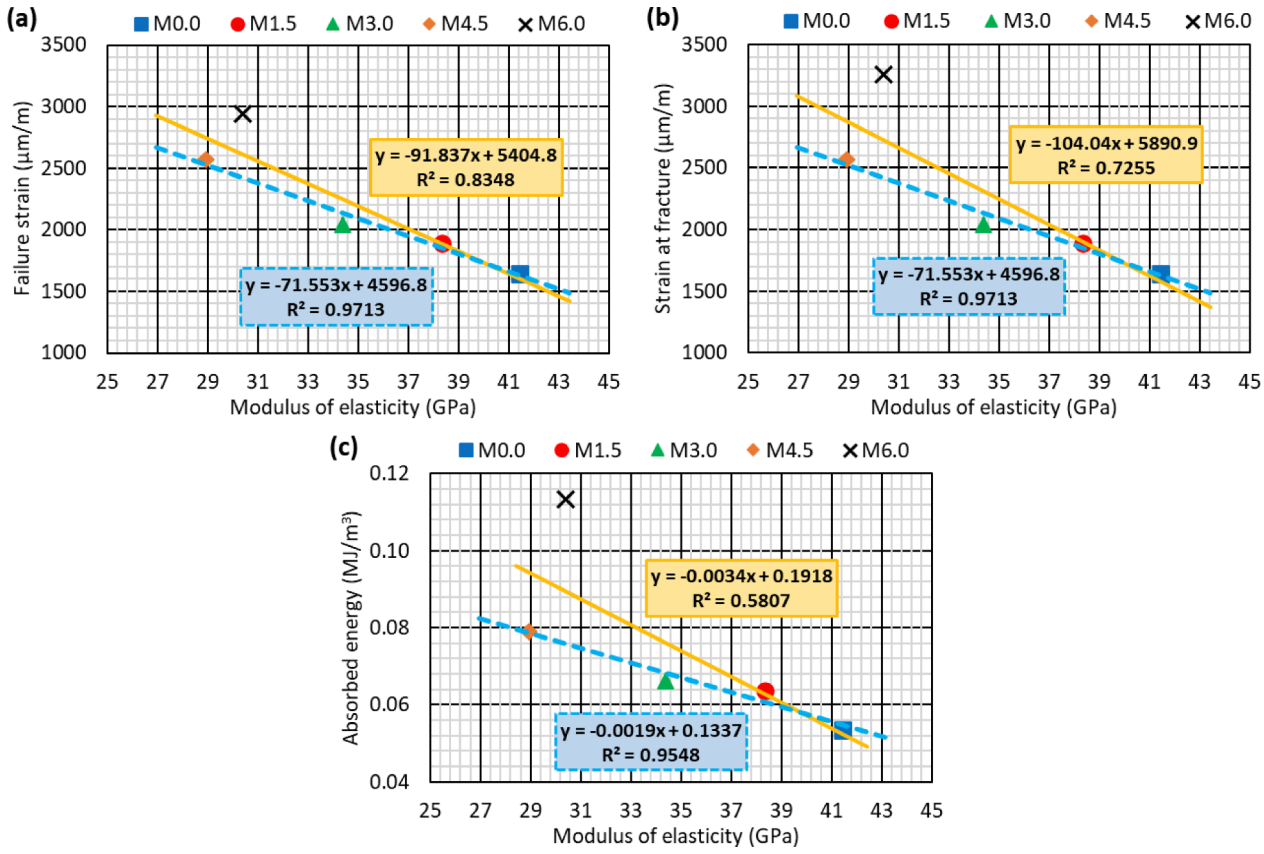

Fig. 5. Longitudinal stress–strain performance under compression. Relationship between the modulus of elasticity and: (a) the failure strain; (b) the fracture strain; (c) the absorbed energy. In all three figures, the dashed blue line represents the regression line of the four mixes containing up to 4.5 % RCTWB, while the continuous yellow line represents the regression line up to 6.0 % RCWTB.

also observed in another study when only the RCWTB fibers, without balsa wood and polyurethane, were added to concrete specimens [37].

3.1.2. Relation between elastic and plastic behavior

The modulus of elasticity is the most commonly used concrete property for the evaluation of concrete deformability levels [50]. The results of analyzing the plastic deformability of concrete containing RCWTB on the basis of its modulus of elasticity are therefore shown in Fig. 5. In each part of the figure, two regression lines are represented. The dashed blue line represents the least squares regression of the results for the mixes with percentage additions equal to or lower than 4.5 % RCWTB. In contrast, the unbroken yellow line represents the regression results for the five concrete mixes containing up to 6 % RCWTB.

For RCWTB contents up to 4.5 % (*M0.0*, *M1.5*, *M3.0* and *M4.5* mixes), a highly accurate linear relationship (R^2 coefficient above 95 %) can be observed between the modulus of elasticity and the three properties that characterize the plastic deformability of concrete: failure strain, fracture strain, and absorbed energy. Therefore, the plastic behavior of concrete under strain can be described according to the elastic stiffness, as described in the conventional models available in the standards [11,12]. A higher modulus of elasticity resulted in lower strain levels within the plastic field and more brittle failures, with lower levels of energy absorbed during the test.

The results for the *M6.0* mix disrupted the direct dependence between the modulus of elasticity and the plastic-deformability values. As mentioned in the previous section, the use of 6.0 % RCWTB meant that the concrete contained sufficient fibers to increase both the modulus of elasticity and the failure strain with respect to the *M4.5* mix, and to increase the fracture strain to higher levels than the failure strain. For this RCWTB content, the stitching effect of the fibers effectively compensated for the discussed negative aspects related to balsa-wood and polyurethane particles. The concrete therefore demonstrated efficient load-bearing capacity and significantly increased the absorbed energy. So, although the elastic stiffness decreased in this concrete mix, all three plastic-deformability values increased, considerably reducing the accuracy of the linear relationship between the elastic modulus and those values. As with conventional fibers, the plastic-deformability approximation applied to plain concrete without fibers was no longer valid when the fiber effect became evident, in this study at percentage additions of 6.0 % RCWTB [13].

3.1.3. Performance prediction

The CEB-FIB model [51] is the most widely known and used among the existing models for estimating the longitudinal stress–strain curve of concrete under compression [52]. It is based on a dimensionless coefficient, K, (Equation (1) that is dependent on the compressive strength, f_c, in MPa, and an initial strain, ε_0, in μm/m (Equation (2) calculated with the modulus of elasticity, E, in GPa and the compressive strength, f_c, in MPa. With the values of both coefficients, the applied stress, σ, may be calculated in MPa as a function of the longitudinal strain, ε, in μm/m as *per* Equation (3). The model applied with no modifications produced estimates to an accuracy of ± 10 % of the longitudinal stress–strain curves of the mixes with percentage additions of up to 4.5 % RCWTB, as shown in Fig. 6a. However, the fit in the compressive-strength vicinity for the *M6.0* mix was very poor, as can also be seen in Fig. 6a. The result was predictable, as the fiber content with that amount of RCWTB effectively improved concrete ductility, as noted from the relationship between the modulus of elasticity and the plastic-deformability values.

$$K = 1 + 2 \times exp(-(f_c/40)) \tag{1}$$

$$\varepsilon_0 = \left(4 + 3 \times K + \sqrt{(4 + 3 \times K)^2 - 40}\right) \times \frac{100 \times f_c}{E} \tag{2}$$

$$\sigma = \frac{f_c \times \left(K \times \varepsilon/\varepsilon_0 - (\varepsilon/\varepsilon_0)^2\right)}{1 + (K - 2) \times \varepsilon/\varepsilon_0} \tag{3}$$

The solution that balanced accuracy and simplicity to reflect the RCWTB fiber effect and for accurate estimation of the longitudinal stress–strain curve under compression of the *M6.0* mix was to define an applied stress, σ', in MPa according to the piecewise function described in Equation (4). Thus, for additions of up to 4.5 % RCWTB, the applied stress, σ', would be equal to the applied stress, σ, provided by the CEB-FIB model [51]. At higher amounts of RCWTB, both applied stresses would also match an applied stress, σ, of 99 % compressive strength. From that point, the applied stress, σ', could be calculated by multiplying the CEB-FIB

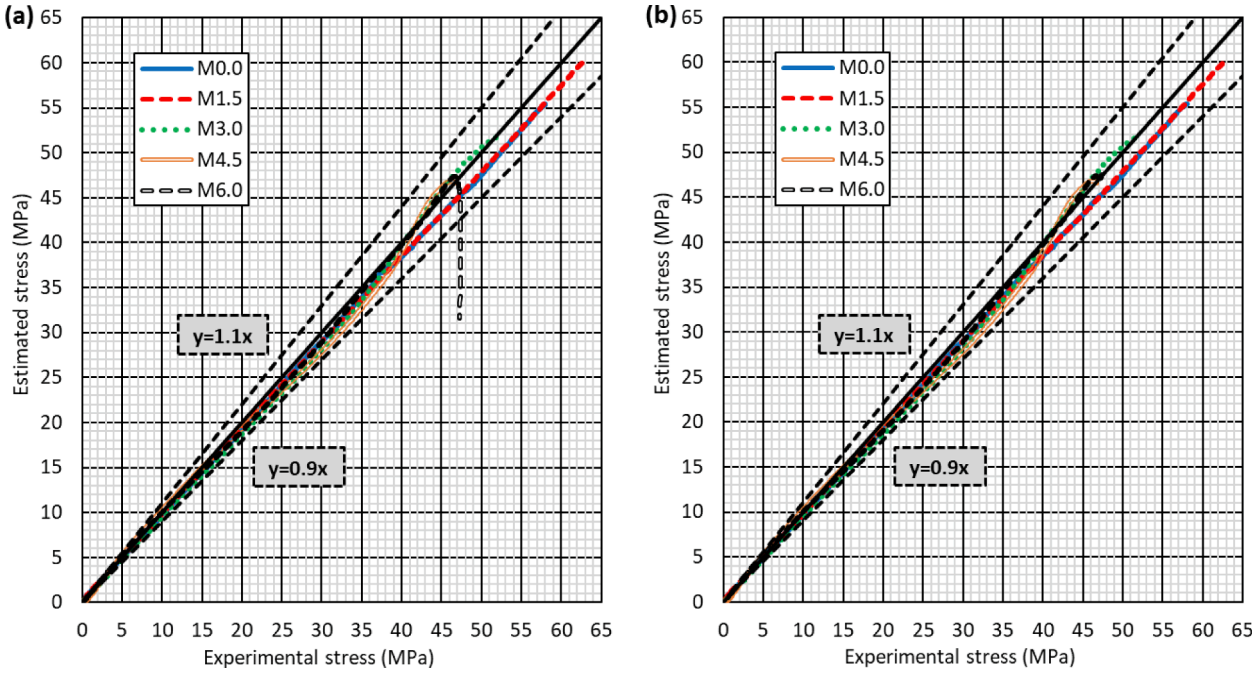

Fig. 6. Comparison of experimental stresses and estimated stresses of the longitudinal stress–strain curve under compression: (a) without model correction; (b) with model correction.

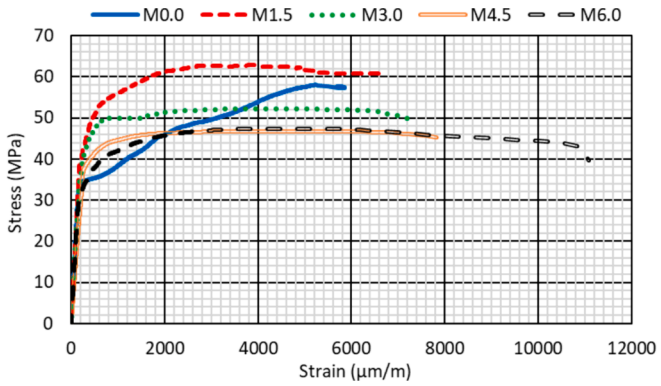

Fig. 7. Transverse stress–strain curves under compression.

applied stress, σ, by an exponential coefficient dependent on the applied stress, σ, itself. The model presented an R^2 coefficient of 99.98 %, so that the stress–strain curve of the five mixes could be estimated to an accuracy of ± 10 %, as shown in Fig. 6b.

$$\sigma' = \begin{cases} \sigma \; if \;\; RCWTB \;\; content \leq 4.5\% \\ \sigma \; if \;\; RCWTB > 4.5\% \;\; and \;\; \sigma \leq 99\% f_c \\ \sigma \times exp\left(2.201 - 0.321 \times \sqrt{\sigma}\right) \;\; in \;\; other \;\; cases \end{cases} \quad (4)$$

3.2. Transverse stress–strain performance under compression

In the deformational-behavior test under compression, the transverse and the longitudinal strain levels were recorded at the same time. The transverse stress–strain curves under compression (Fig. 7) and their key values (Table 4) could then be calculated.

The transverse stress–strain curves showed the usual shape [13]. Thus, an elastic zone with much smaller strain levels than in the longitudinal direction was initially detected, after which a plastic zone was observed. That plastic zone started with a yield step caused by vertical-splitting cracking in the *M0.0* mix. However, that zone was not identified in the other mixes, so it was thought that the fiber stitching effect in the RCWTB prevented vertical-splitting cracking, in the same way as commercial fibers can prevent it [13]. The use of minimal RCWTB amounts meant that sufficient fibers were available to withstand any sharp increase in strain, common to all types of non-fiber-reinforced concretes [7], as shown for example in Fig. 1.

Several effects of RCWTB in relation to the transverse deformability of the concrete specimens under compression are shown in Table 4:

- Transverse deformability within the elastic zone, shown by the Poisson's coefficients (5.0 % lower in the *M6.0* mix than in the *M0.0* mix), decreased with higher percentage additions of RCWTB. The RCWTB-fiber stitching effect within the cementitious matrix therefore decreased specimen bulging during the test [14]. However, additions of 1.5 % RCWTB contained insufficient fiber amounts to replicate that effect. As happened in the longitudinal direction, the strain at the limit of proportionality showed no clear trend with larger amounts of RCWTB.
- The addition of RCWTB always reduced the failure strain with respect to the *M0.0* mix, presumably due to the absence of the abrupt increase in strain caused by the yield step [7]. However, the higher the waste content, the smaller the decrease (25.9 % for the *M1.5* mix and 12.0 % for the *M6.0* mix), as shown in Fig. 8a. The ductility of concrete increased due to the RCWTB-fiber stitching effect, and it was perhaps the reason for the cracking due to the weak interfacial transition zones generated by surrounding the particles of balsa wood and polyurethane to be almost imperceptible [49].

Table 4
Key values of the transverse stress–strain behavior under compression.

Property	Parameter	*M0.0*	*M1.5*	*M3.0*	*M4.5*	*M6.0*
Poisson's coefficient	**Value**	0.202	0.206	0.196	0.192	0.192
	Δ RCWTB content (%)	0.0	1.9	−2.9	−4.8	−4.9
Strain at the limit of proportionality	**Value (μm/m)**	167	209	193	220	176
	Δ RCWTB content (%)	0.0	25.1	15.6	31.7	5.4
Compressive strength (failure stress)	**Value (MPa)**	58.0	62.8	52.2	46.8	47.4
	Δ RCWTB content (%)	0.0	8.3	−10.0	−19.3	−18.3
Failure strain	**Value (μm/m)**	5231	3875	4135	4393	4601
	Δ RCWTB content (%)	0.0	−25.9	−21.0	−16.0	−12.0
Strain at fracture	**Value (μm/m)**	5706	6720	7253	7815	11,091
	Δ RCWTB content (%)	0.0	17.8	27.1	37.0	94.4
Absorbed energy	**Value (MJ/m^3)**	0.2716	0.3961	0.3641	0.3526	0.4975
	Δ RCWTB content (%)	0.0	45.8	34.1	29.8	83.2

'**Δ RCWTB content (%)**' refers to the percentage variation with respect to the *M0.0* reference mix.

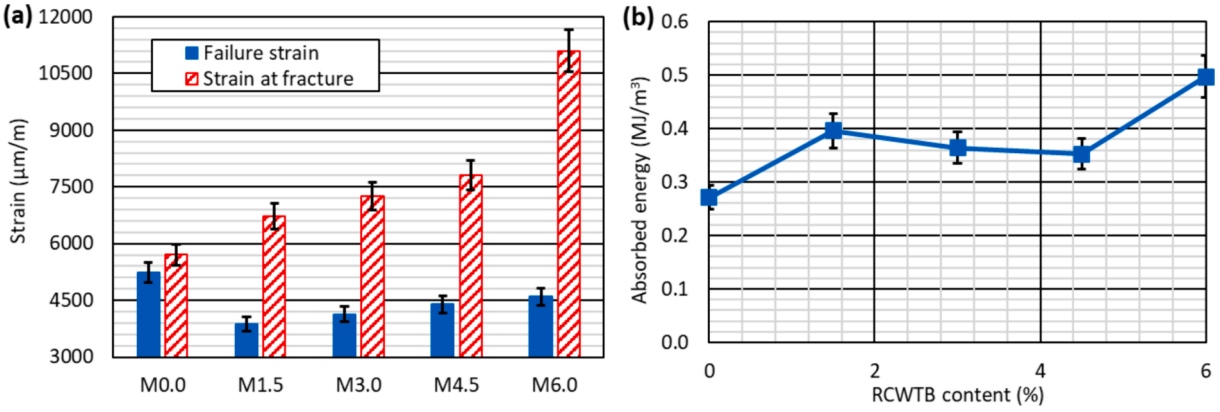

Fig. 8. Transverse stress–strain performance under compression: (a) comparison between failure strain and fracture strain; (b) evolution of absorbed energy with RCWTB content.

- Higher percentage additions of RCWTB implied higher concrete ductility that was also evident as the fracture strain increased (Fig. 8a). In fact, the fracture strain of the *M6.0* mix was almost twice that of the *M0.0* mix (11091 μm/m vs. 5706 μm/m). Furthermore, the higher the RCWTB content, the greater the fracture strain compared to the failure strain, and therefore the stronger the load-bearing capacity [18]. Consequently, the RCWTB mixes had higher levels of absorbed energy than the *M0.0* mix (Fig. 8b), although the levels of absorbed energy remained constant at additions between 1.5 % and 4.5 %. RCWTB. The *M6.0* mix had by far the highest levels of absorbed energy, 83.2 % higher than the *M0.0* mix, due to the increased strain at fracture [13].

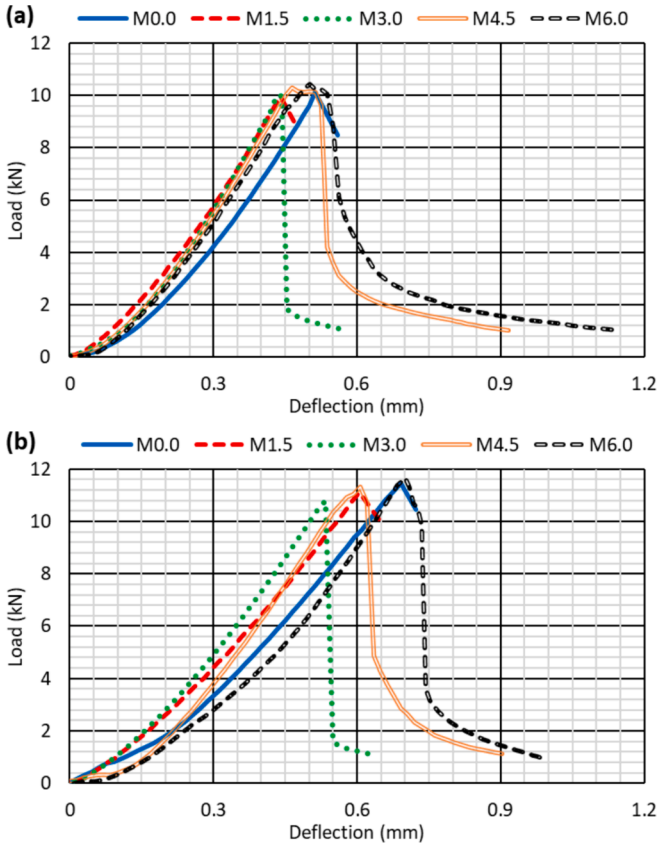

Fig. 9. Load-deflection curves under bending: (a) 7 days; (b) 90 days.

3.3. Deflection performance under bending forces

The test press continuously recorded the deflection behavior under bending, registering applied load and piston displacement at the center of the specimen [13]. The results were used to generate the load–deflection curves, shown in Fig. 9, and their key values, detailed in Table 5. The stronger load-bearing capacity due to the fiber effect is mainly detected in the bending behavior [19,21,27]. The test was therefore performed at 7 and at 90 days to evaluate the changes to that capacity over time, from a very early age to an age at which the mechanical behavior of the concrete was thought to have stabilized [7].

The curves had standard shapes [8]. Initially curved, due to the adjustment of the specimen to the loading piston, and then linear between the applied load and the deflection up until to the point of failure. Furthermore, the mixes containing percentage additions equal to or higher than 3.0 % RCWTB were able to withstand loading after the failure point. All those aspects are discussed in detail in the following subsections.

3.3.1. Analysis of pre-failure performance

The pre-failure bending behavior of concrete is characterized by the compliance of the material, which is the inverse of the slope of the linear zone of the load–deflection curve [17]. It can be expressed in mm/kN and it reflects the deflection of the concrete specimen as the load increases. The compliance values of all the mixes at both ages were calculated with the data in Fig. 9 and are detailed in Table 5.

The effect of RCWTB on concrete compliance was different at 7 and at 90 days. In general, 7-day compliance increased proportionally with the RCWTB content. With respect to the *M0.0* mix (0.0305 mm/kN), the compliance increased by 1.8 % in the *M1.5* mix (0.0310 mm/kN) and by 16.7 % in the *M6.0* mix (0.0356 mm/kN). This behavior was closely linked to the modulus of elasticity (Table 5), there being an inversely proportional relation between both properties, as shown in Fig. 10a, which reflects the results based on the theory of Strength of Materials [53]. Thus, the decrease in the elastic modulus caused by RCWTB led in

Table 5
Key values of the load–deflection behavior under bending.

Property	Parameters	7 days					90 days				
		M0.0	*M1.5*	*M3.0*	*M4.5*	*M6.0*	*M0.0*	*M1.5*	*M3.0*	*M4.5*	*M6.0*
Modulus of elasticity	**Value (GPa)**	38.2	35.2	31.5	26.1	28.2	41.4	38.4	34.4	28.9	30.4
	Δ RCWTB content (%)	0.0	−7.9	−17.7	−31.7	−26.3	0.0	−7.4	−17.0	−30.1	−26.6
	Δ 7–90 days (%)	–	–	–	–	–	8.4	8.9	9.3	10.9	7.9
Compliance	**Value (mm/kN)**	0.0305	0.0310	0.0330	0.0343	0.0356	0.0594	0.0480	0.0380	0.0384	0.0406
	Δ RCWTB content (%)	0.0	1.8	8.3	12.6	16.7	0.0	−19.2	−36.1	−35.3	−31.6
	Δ 7–90 days (%)	–	–	–	–	–	94.7	54.7	14.9	11.8	14.1
Flexural strength (failure stress)	**Value (MPa)**	5.39	5.33	5.34	5.48	5.57	6.12	5.97	5.88	6.06	6.22
	Δ RCWTB content (%)	0.0	−1.1	−1.0	1.7	3.4	0.0	−2.5	−3.9	−1.0	1.6
	Δ 7–90 days (%)	–	–	–	–	–	13.5	11.9	10.2	10.6	11.6
Failure deflection	**Value (mm)**	0.52	0.55	0.43	0.46	0.50	0.69	0.61	0.53	0.61	0.70
	Δ RCWTB content (%)	0.0	5.8	−17.3	−11.5	−3.8	0.0	−11.6	−23.2	−11.6	1.4
	Δ 7–90 days (%)	–	–	–	–	–	32.7	10.9	23.3	32.6	40.0
Stress at fracture	**Value (MPa)**	4.52	4.77	0.55	0.55	0.56	5.57	5.27	0.59	0.61	0.52
	Δ RCWTB content (%)	0.0	5.7	−87.9	−87.7	−87.6	0.0	−5.5	−89.4	−89.1	−90.6
	Δ 7–90 days (%)	–	–	–	–	–	23.4	10.3	8.1	9.8	−6.9
Deflection at fracture	**Value (mm)**	0.56	0.47	0.58	0.92	1.14	0.72	0.65	0.63	0.90	0.98
	Δ RCWTB content (%)	0.0	−16.1	4.3	63.5	102.7	0.0	−9.7	−13.2	24.8	36.0
	Δ 7–90 days (%)	–	–	–	–	–	29.1	38.9	7.6	−1.4	−13.4
Absorbed energy	**Value (mm·kN)**	2.41	2.11	2.01	3.33	3.99	3.45	3.44	2.65	3.61	3.78
	Δ RCWTB content (%)	0.0	−12.1	−16.6	38.6	66.0	0.0	−0.3	−23.2	4.8	9.7
	Δ 7–90 days (%)	–	–	–	–	–	43.2	62.5	31.9	8.3	−5.3

'**Δ RCWTB content (%)**' refers to the percentage variation with respect to the *M0.0* reference mix at each age.
'**Δ 7–90 days (%)**' refers to the percentage variation of the 90-day value of each mix with respect to the 7-day value of the same mix.

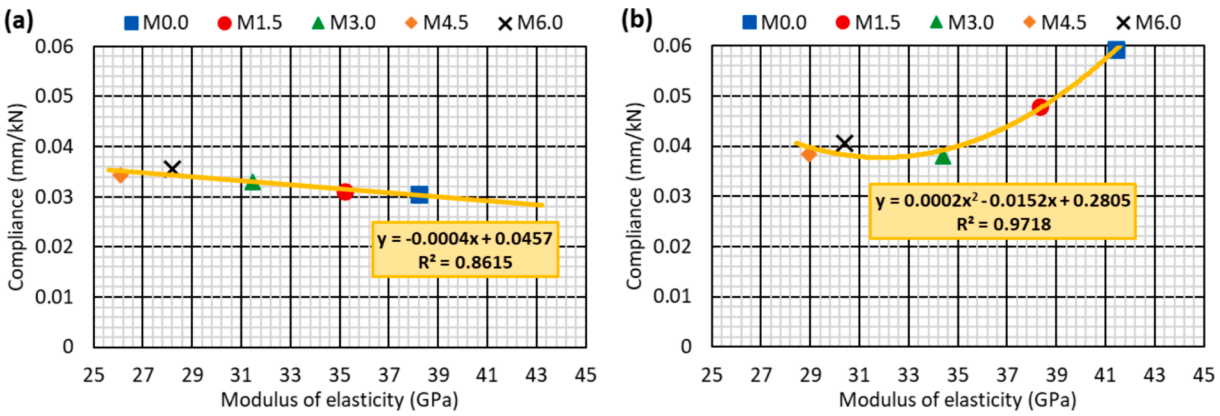

Fig. 10. Deflection performance under bending. Relation between modulus of elasticity and compliance: (a) 7 days; (b) 90 days.

turn to higher compliance values at 7 days and higher bending deformability in the linear zone of the load–deflection curve at this age.

Although the modulus of elasticity at 90 days had also decreased in proportion with the percentage additions of RCWTB, compliance was reduced with additions of up to 3.0 %, after which it slightly increased. The relationship between the modulus of elasticity and compliance at 90 days was therefore a second-degree polynomial, as shown in Fig. 10b. The modulus of elasticity conditioned concrete stiffness within the compressed zone during the deflection-behavior test [53], while the RCWTB fibers conditioned stiffness within the zone under tension:

- At 7 days, adhesion between the cementitious matrix and the RCWTB fibers was low, so the stitching effect in the tension zone was weak and the fibers were unable to withstand the increase in concrete deflection, because of the reduction in the modulus of elasticity after the RCWTB was added [54].
- Low percentage additions of RCWTB effectively reduced concrete deformability under bending stresses at 90 days, due to higher adherence levels between the cementitious matrix and the fibers, making the RCWTB stitching effects more noticeable and compensating for the lower modulus of elasticity (decrease of 19.2 % for the *M1.5* mix with respect to the *M0.0* mix) [55]. Nevertheless, rather than a reduction in compliance with additions of more than 3.0 % RCWTB, compliance slightly increased, due to the decrease in the modulus of elasticity (compliance decreases of 36.1 % and 31.6 % for the *M3.0* and *M6.0* mixes regarding the *M0.0* mix, respectively) [8].

Finally, compliance increased with age in all the mixes, perhaps due to their higher brittleness and the greater tendency of concrete to crack at older ages [25]. However, the higher the percentage additions of RCWTB, the lower the increase in compliance, due to the stitching effect of the RCWTB fibers.

3.3.2. *Analysis of the failure point*

Both the flexural strength and the failure deflection [21], which characterized the failure point, are shown in Table 5.

The 7-day flexural strength remained constant for RCWTB contents between 0.0 % and 3.0 %, and slightly increased at higher contents (3.4 % increase for the *M6.0* mix with respect to the *M0.0* mix). Although the RCWTB-fiber stitching effect never reduced concrete compliance at early ages, they did increase flexural strength [55]. The behavior at 90 days was similar, although only the *M6.0* mix showed a slightly higher flexural strength than the reference mix. In any case, all strength variations were reduced, less than 4.0 % in percentage terms. The strength increases between 7 and 90 days showed no dependency on the percentage additions of RCWTB.

The failure-deflection trends were also similar at both ages, decreasing with additions of up to 3.0 % RCWTB (deflection 17.3 % lower at 7 days and 23.2 % lower at 90 days than the *M0.0* mix), after which it increased, so that the *M6.0* mix showed almost the same failure deflections as those of the reference mix (variations lower than 4.0 % with regard the *M0.0* mix). From an intuitive point of view, it could be thought that higher compliance should equate with higher failure deflection [17]. As shown in Fig. 11a, that premise was true in the RCWTB concrete mixes, although it was not a very precise relation, as the failure deflection was also conditioned the initial zone of the load–deflection curve and the compliance variations in absolute terms were low. On the other hand, the flexural strength of the mixes defines the extent of the linear zone of the load–deflection curve [37]. In fact, flexural strength and failure strain presented the most accurate relation, as depicted in Fig. 11b, mainly because both properties showed similar trends and a clear proportionality. Therefore, the failure deflection was

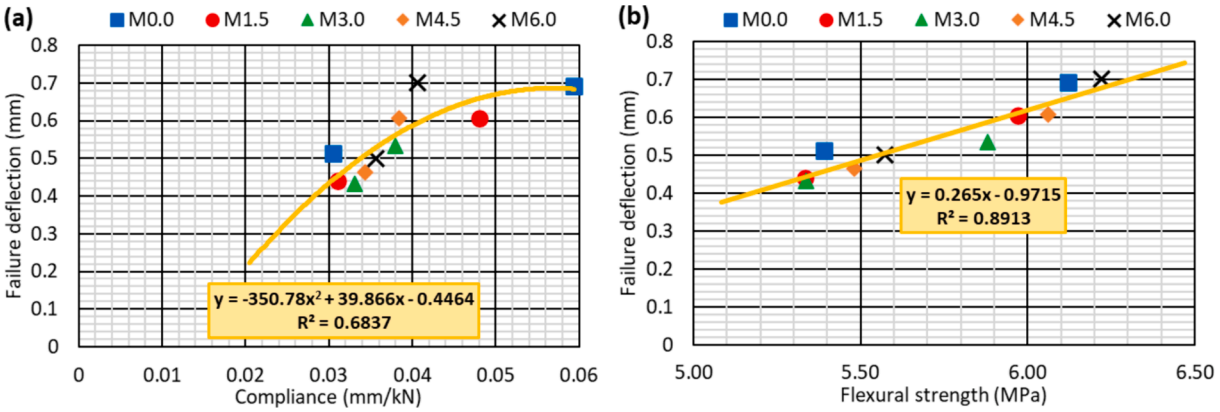

Fig. 11. Deflection performance under bending. Failure deflection as a function of: (a) compliance; (b) flexural strength.

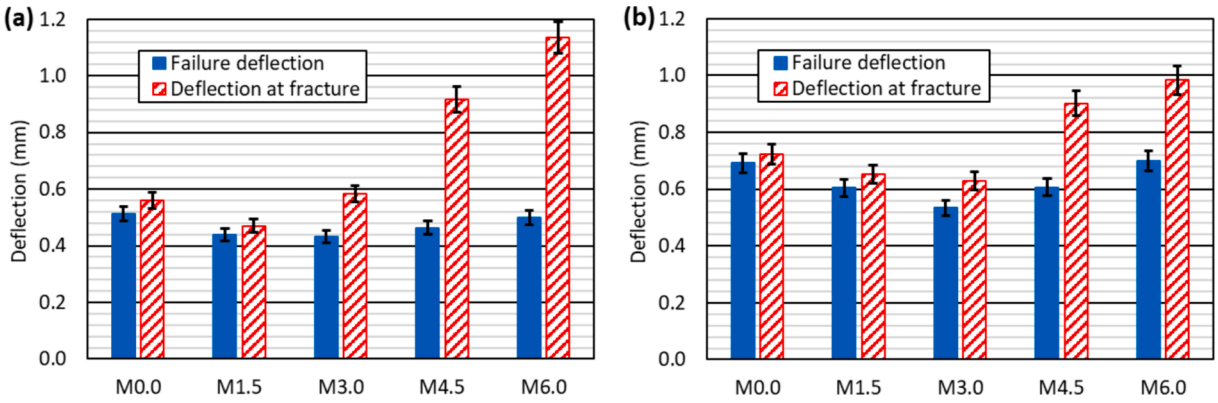

Fig. 12. Deflection performance under bending. Comparison of failure and fracture deflections at: (a) 7 days; (b) 90 days.

mainly conditioned by the ultimate strength of concrete (flexural strength), and not so much by the slope of the linear zone of the load–deflection curve, whose inverse is the compliance. Failure deflection increased with age in all the mixes, as did compliance, presumably due to increased initial micro-cracking to adapt to the load [8].

3.3.3. Analysis of load-bearing capacity

Conventionally, brittle breakage of concrete occurs when it reaches the failure point under bending stresses and is unable to support any further loading [19]. However, the fiber additions strengthen the load-bearing capacity of the concrete specimens, so that the applied load decreases progressively as deflection increases [18]. Although the presence of balsa-wood and polyurethane particles reduced the ultimate deflection, their influence was null after failure, with fibers being the only RCWTB component that affected the flexural behavior of the concrete after that point. The fibers therefore stitched the cracks after the failure, thus strengthening the load-bearing capacity of the concrete within percentage additions of 3.0 % or more RCWTB, as the fracture values in Table 5 and the load–deflection curves in Fig. 9 might suggest.

The *M0.0* and *M1.5* mixes showed very similar values for failure deflection and deflection at fracture at both ages (Fig. 12), with differences of around 0.04 mm. Moreover, their fracture-stress values were only 0.50 MPa lower than their failure-stress values (Fig. 13). Both aspects were indicative of the brittle failure that those concrete mixes underwent [20]. The stress at fracture of the other three mixes was 0.50–0.60 MPa at both ages, although their flexural strengths were always higher than 5.0 MPa (Fig. 13). Those mixes supported load after failure, which progressively decreased as the deflection increased (Fig. 9). In Fig. 12, the deflection at fracture is shown to be between 0.10–0.15 mm greater than the failure deflection for the *M3.0* mix, while the *M4.5* and *M6.0* mixes showed post-failure deflection increases of at least 0.30 mm, which represented approximately 50 % of the failure deflection. The higher increase in post-failure deflection in the mixes with higher RCWTB amounts meant that the load decreased more slowly, making the RCWTB-fiber stitching effects more noticeable [13,21]. Sudden and unexpected failure of a concrete structure containing RCWTB could therefore be avoided, and evacuation times lengthened [25].

The trends for deflection at fracture and failure deflection of the RCWTB specimens were very similar. Thus, compared to the *M0.0* mix, fracture deflection decreased when 1.5 % RCWTB was added, remaining approximately constant at 3.0 % RCWTB, and increasing at higher percentage additions. Regarding the time factor, the deflection at fracture had increased between 7 and 90 days for percentage additions between 0.0 % and 3.0 % of RCWTB, due to the influence of the failure deflection. However, the 1.4 % and the 13.4 % decreases for the *M4.5* mix and the *M6.0* mix, respectively, were probably due to increased adhesion between the cementitious matrix and the RCWTB fibers [24,27], which limited the post-failure deformability of the mix in much the same way as compliance. Stress at fracture at percentage additions of over 3.0 % RCWTB remained approximately constant, regardless of age. Given the variations of flexural strength (Table 5), the aforementioned aspects caused the absorbed energy to decrease with percentage additions of up to 3.0 % RCWTB, after which the absorbed energy increased at higher additions. In the same way, at higher percentage additions of RCWTB, the lower increase of absorbed energy between 7 and 90 days was due to the temporal reduction of deflection at fracture. Once again, the reason might be the increased adhesion of the RCWTB fibers to the cementitious matrix at advanced ages [27].

3.3.4. Pre-failure performance prediction

The estimation of the load–deflection curve of fiber-reinforced concrete has also been reported in the scientific literature. In general, the estimation of the post-failure behavior requires the use of advanced

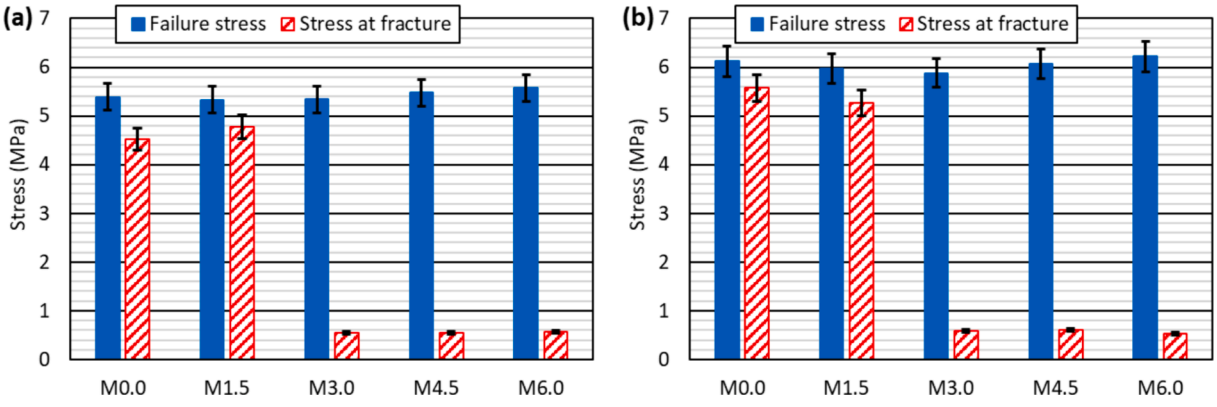

Fig. 13. Deflection performance under bending. Comparison of the failure stress and the stress at fracture: (a) 7 days; (b) 90 days.

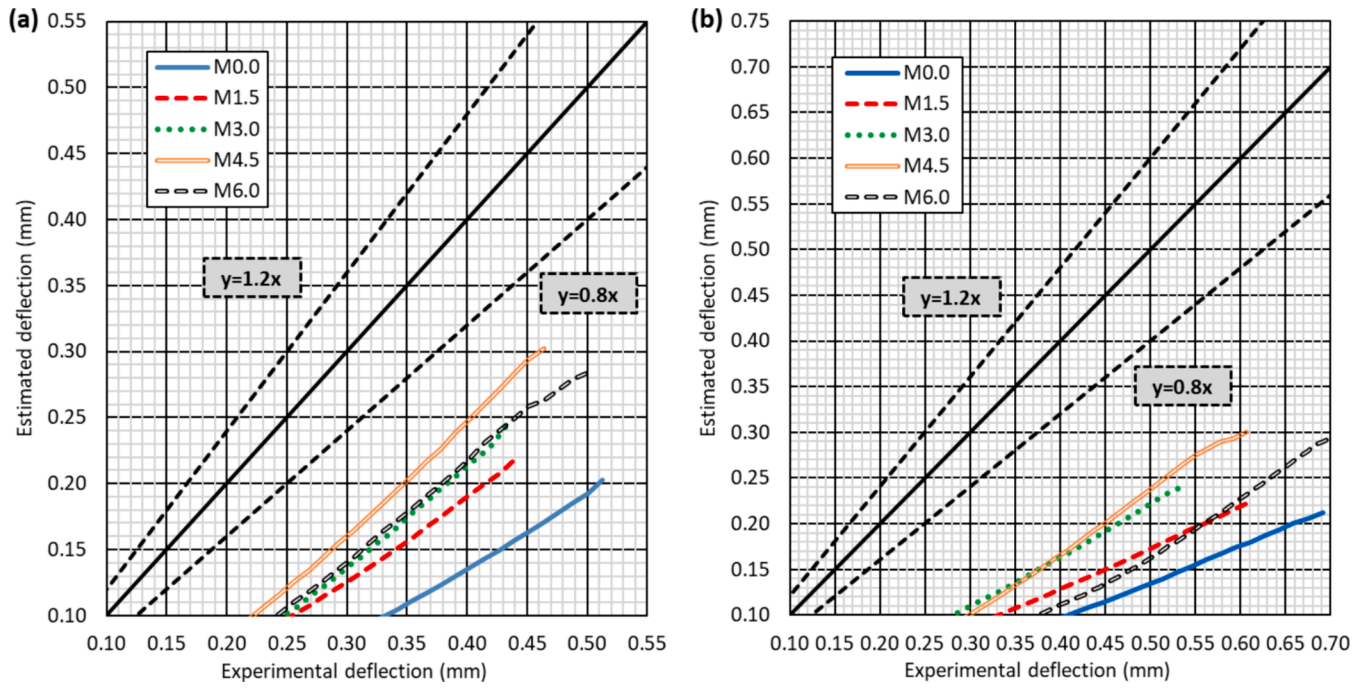

Fig. 14. Comparison of the experimental deflections of the load–deflection curve under bending and the deflections estimated with the non-modified conventional model (Equation (5)): (a) 7 days; (b) 90 days.

tools, such as the finite element method, which require specific inputs such as data on tensile strength [56]. However, the pre-failure behavior, more specifically the linear zone of the load–deflection curve defined by compliance, can be estimated in simpler ways with the Strength of Materials theory and its formulas [53].

Equation (5) shows the formula for estimating the pre-failure deflection, D, in mm, as a function of the applied load, L, in kN, and the modulus of elasticity, E, in kN/m^2. In this formula, the arrangement of supports and load points of a concrete specimen in a four-point flexural-strength test and the dimensions of the 75 × 75 × 275-mm prismatic specimens (75-mm width, 75-mm height, 225-mm span) are specified. It also includes a coefficient to consider the effect of concrete cracking. Experimental deflection was underestimated in the results of the model, as can be appreciated in Fig. 14. However, a linear relationship is also shown in that figure between the experimental and the estimated deflections. It could therefore be stated that the problem with the model in Equation (5) was the assumption of a higher bending stiffness than the actual one, which led to an underestimation of the concrete compliance value.

$$D = 766666.7 \times \frac{L}{E} \tag{5}$$

Based on the above and seeking a balance between ease of calculation and estimation accuracy, the modified model shown in Equation (6) was developed. This model simply consisted of the basic model in Equation (5), multiplied by a dimensionless coefficient, C, calculated with Equation (7) and Equation (8), using the test results at 7 and 90 days, respectively. The objective of the coefficient C was to modify the concrete compliance in Equation (5), so it was statically defined on the basis of the aspects discussed in the section related to the pre-failure behavior. Thus, on the one hand, formulas were developed that depended on the modulus of elasticity of the concrete at each age (E_7, 7-day modulus of elasticity in GPa, and E_{90}, 90-day modulus of elasticity in GPa). Furthermore, the formulas were adjusted to the relation between modulus of elasticity and compliance at both ages (Fig. 10): an inverse linear relationship at 7 days and a second-degree polynomial relationship at 90 days. The use of that correction coefficient was enough to estimate the pre-failure deflection of the concrete mixes in the linear zone of the load–deflection curve, once the initial curved zone had been exceeded, to an accuracy of ± 20 %, as shown in Fig. 15.

$$D = C \times 766666.7 \times \frac{L}{E} \tag{6}$$

$$C_7 = \frac{1}{1.056 - 0.018 \times E_7} \tag{7}$$

$$C_{90} = 12.233 - 0.637 \times E_{90} + 0.010 \times {E_{90}}^2 \tag{8}$$

3.4. Deformational performance under indirect-tensile stresses

The deflection-behavior test was complemented with a deformational-performance test under indirect-tensile stress, to investigate the effectiveness of the RCWTB-fiber stitching effect at strengthening load-bearing capacity. Thus, a splitting-tensile-strength test was conducted, but with continuous recording of the indirect-tensile stress and the displacement of the loading piston. The specimen broke in its entirety under tensile stress at the failure point of this test, so there was no zone in the concrete specimen that kept working under compression, in the same way than in the deflection-behavior test [44]. Fibers were therefore the only elements that were able to support loading after failure. High percentage additions of fibers with an optimal adherence to the cementitious matrix are needed to reach that performance [55]. The deformational curves that reflect the test results and the key values are respectively shown in Fig. 16 and Table 6.

All the deformational curves showed a perfectly straight line up to the failure point. That zone was characterized by two properties:

- On the one hand, the splitting tensile strength, which remained approximately constant at percentage additions between 0.0 % and 3.0 % RCWTB and decreased by around 8.0 % at higher amounts. Results that were thought to have been conditioned by the effect of the water/cement ratio on the bond between the cementitious matrix and the aggregate [44]. Thus, the effect of the fibers at percentage additions of up to 3.0 % RCWTB compensated for the negative effect

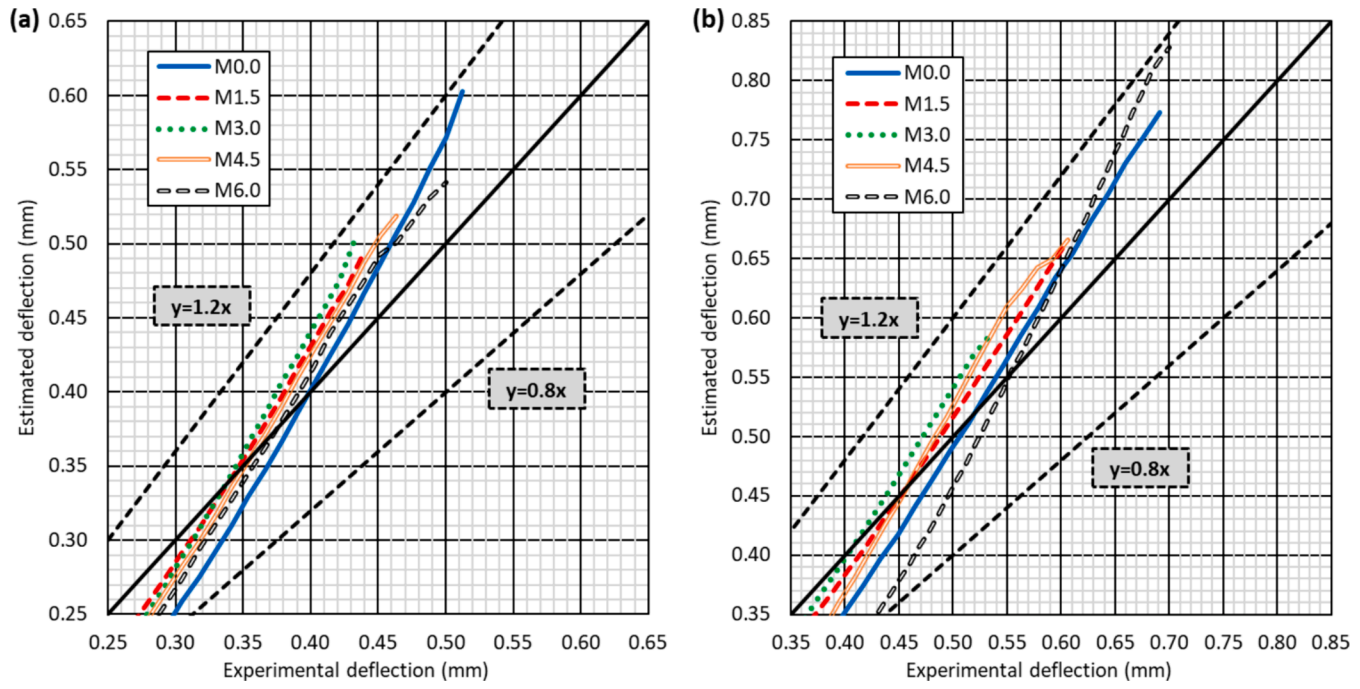

Fig. 15. Comparison of the experimental deflections of the load–deflection curve under bending and the deflections estimated with the developed model (Equation (6)): (a) 7 days; (b) 90 days.

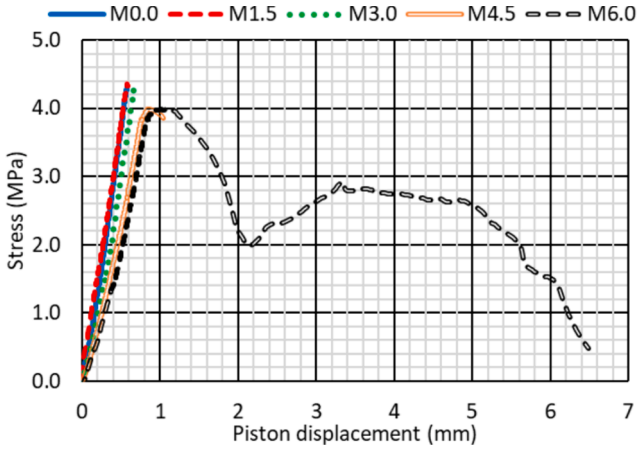

Fig. 16. Deformational curves under indirect-tensile stresses.

of higher water/cement ratios (Table 2) [13]. Nevertheless, the increase in this ratio was critical at percentage additions of 4.5 % RCWTB, which prompted a sharp decrease in this strength. Higher percentage additions of 6.0 % RCWTB (*M6.0* mix) led to the same behavior as above, where the RCWTB-fiber stitching effect compensated the effect of an increased water/cement ratio.

- On the other hand, tensile deformability, the inverse of the slope of the linear zone, recorded in terms of loading piston displacement *per* MPa of indirect-tensile stress applied. The increased additions of RCWTB also increased the deformability of the concrete under that type of stress. Thus, the *M6.0* mix presented a tensile deformability that was 34.0 % higher than that of the reference concrete. This performance could be due to the increase in the water/cement ratio with the increase in the content of this waste, as well as to the presence of RCWTB balsa-wood and polyurethane particles [7,46]. A very precise inverse linear dependence between the splitting tensile strength and the tensile deformability was observed in the mixtures (Fig. 17a), so that a higher value of one property resulted in a lower value of the other and *vice versa*.

As can be noted in Fig. 16, the failure in the concrete mixes with percentage additions of 3.0 % RCWTB was sudden, so that the mixes were unable to support load after it. The *M4.5* mix showed a slight load-bearing capacity, so that there was no abrupt curve ending at the failure point. However, a load piston displacement of 5.5 mm was detected from the failure point to fracture in the *M6.0* mix, which showed a large load-bearing capacity because the addition of 6.0 % RCWTB provided a sufficient fiber content in the concrete to reach this performance. In addition, a post-failure zone was also recorded, in which the load supported by the specimen increased. This zone is usually found when metallic fibers are used [13]. Its appearance in this study demonstrated adequate adhesion between the RCWTB fibers and the cementitious matrix and the high tensile strength of the fibers [19,28]. Absorbed energy and tensile deformability both increased in a linear relation, as there were no large splitting tensile strength variations up to percentage additions of 4.5 % RCWTB (dashed blue line, Fig. 17b). The fiber

Table 6
Key values of the deformational behavior under indirect-tensile stresses.

Property	Parameters	*M0.0*	*M1.5*	*M3.0*	*M4.5*	*M6.0*
Splitting tensile strength (failure stress)	**Value (MPa)**	4.33	4.35	4.27	3.99	3.97
	Δ RCWTB content (%)	0.0	0.5	−1.4	−7.9	−8.3
Tensile deformability	**Value (mm/MPa)**	0.1335	0.1329	0.1449	0.1714	0.1789
	Δ RCWTB content (%)	0.0	−0.4	8.5	28.4	34.0
Absorbed energy	**Value (mm·MPa)**	1.18	1.34	1.27	2.39	15.73
	Δ RCWTB content (%)	0.0	13.6	7.6	102.5	1233.1

'**Δ RCWTB content (%)**' refers to the percentage variation with respect to the *M0.0* reference mix.

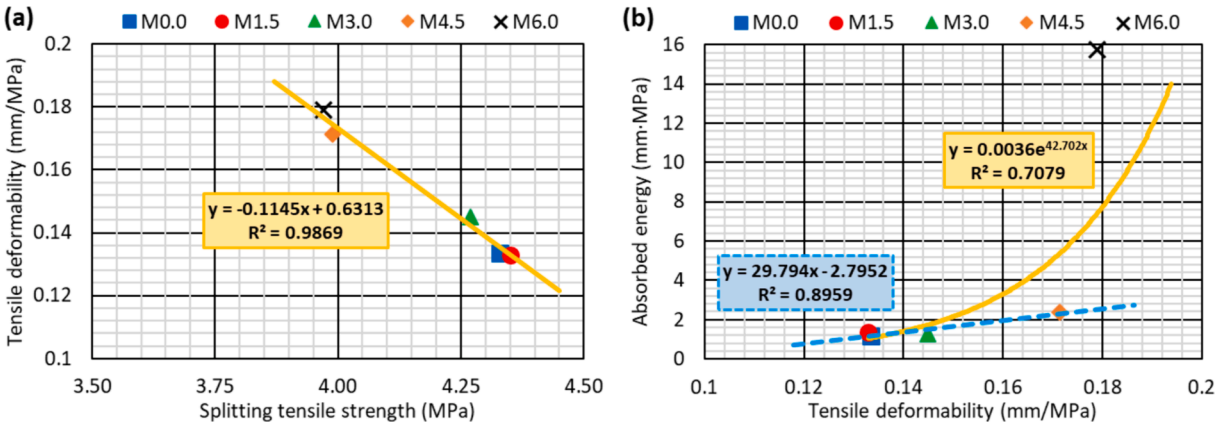

Fig. 17. Deformational performance under indirect-tensile stresses: (a) relationship between splitting tensile strength and tensile deformability; (b) relationship between tensile deformability and absorbed energy, in which the dashed blue line means the regression line up to 4.5 % RCWTB and the solid yellow line represents the repression line up to 6.0 % RCWTB.

Table 7
Absorbed energy *per* unit of strength.

	M0.0	*M1.5*	*M3.0*	*M4.5*	*M6.0*
Longitudinal stress–strain behavior (MJ/(m^3·MPa))	0.0009	0.0010	0.0013	0.0017	0.0024
Transverse stress–strain behavior (MJ/(m^3·MPa))	0.0047	0.0063	0.0070	0.0075	0.0105
7-day deflection behavior ((mm·kN)/MPa)	0.4471	0.3959	0.3764	0.6077	0.7163
90-day deflection behavior ((mm·kN)/MPa)	0.5637	0.5762	0.4507	0.5957	0.6077
Deformational indirect tensile behavior ((mm·MPa)/MPa)	0.2725	0.3080	0.2974	0.5990	3.9622

Table 8
Carbon footprint and absorbed energy *per* unit of carbon footprint.

	M0.0	*M1.5*	*M3.0*	*M4.5*	*M6.0*
Carbon footprint (kg CO_2 eq/m^3)	306.7	300.9	295.1	289.3	284.5
Longitudinal stress–strain behavior (MJ/kg CO_2 eq)	0.00017	0.00021	0.00022	0.00027	0.00040
Transverse stress–strain behavior (MJ/kg CO_2 eq)	0.00089	0.00132	0.00123	0.00122	0.00175
7-day deflection behavior ((mm·kN)/(kg CO_2 eq/m^3))	0.00786	0.00701	0.00681	0.01151	0.01403
90-day deflection behavior ((mm·kN)/(kg CO_2 eq/m^3))	0.01125	0.01143	0.00898	0.01248	0.01329
Deformational indirect-tensile behavior ((mm·MPa)/(kg CO_2 eq/m^3))	0.00385	0.00445	0.00430	0.00826	0.05530

stitching effect in the *M6.0* mix resulted in a huge increase in the absorbed energy, 10 times higher than that of the *M0.0* mix, so the evolution of the absorbed energy considering this RCWTB content was approximately exponential.

3.5. Summary: absorbed energy per unit of strength and carbon footprint

As observed throughout the study, the use of RCWTB strengthened load bearing capacity and increased concrete ductility, although in some cases it also reduced the strength of the concrete specimens. Thus, one aspect could compensate for the other. Absorbed energy is the quintessential magnitude for comparing the ductility of a material subjected to a continuous-load-to-failure test, including concrete [46,56]. If this energy is calculated *per* unit of strength, a value of ductility is obtained that can be compared between different materials or concrete mixes disregarding the mechanical strength. The energy absorbed *per* unit of strength for all the tests is shown in Table 7. That value can generally be seen to increase with the use of RCWTB. Percentage additions of RCWTB were therefore effective at increasing the energy absorbed by the concrete under all loading conditions, despite the eventual decrease in strength that it sometimes caused.

The carbon footprint of the concrete mixes *per* m^3 can be calculated on the basis of their composition (Table 2) plus the carbon footprint of their components as reported in the literature [57–59]. The carbon footprint of the mixes is detailed in Table 8. The use of RCWTB reduced the carbon footprint, due to the decrease in cement content *per* m^3, the component with the highest carbon footprint [41]. The energy absorbed *per* unit of carbon footprint in general increased with additions of RCWTB, an aspect that is also reflected in Table 8, which shows that the use of this waste material increased the ductility of concrete while reducing its negative environmental consequences.

4. Conclusions

The potential of Raw-Crushed Wind-Turbine Blade (RCWTB) to increase concrete ductility and the potential of its GFRP-composite fibers to strengthen load-bearing capacity have both been analyzed in this study. Thus, concrete mixes with RCWTB contents of 0.0 %, 1.5 %, 3.0 %, 4.5 %, and 6.0 % by volume were prepared and subjected to different tests to analyze their 90-day longitudinal and transverse stress–strain performance under compression, their 7- and 90-day deflection behavior under bending, and their 90-day deformational behavior under indirect-tensile stresses. The test results yielded the following conclusions:

- Higher percentage additions of RCWTB increased the longitudinal failure strain of the specimens under compression. However, the mix with a percentage addition of 6.0 % RCWTB was the only mix to show a higher fracture than failure strain, meaning that it could support loading from the point of failure and demonstrating a large increase in absorbed energy. All the magnitudes characterizing the ductile behavior of concrete in the longitudinal direction were

linearly related to the modulus of elasticity of the concrete specimens up to percentage additions of 4.5 % RCWTB, as higher amounts increased the fiber content until it was sufficient for the fiber stitching effect to condition the longitudinal stress–strain behavior of the concrete specimens.

- The RCWTB-fiber stitching effect reduced both the transverse elastic deformability under compression and the failure strain of the specimens. That same effect also suppressed the yield step due to vertical-splitting cracking after the elastic zone. However, both the strain at fracture and the difference between failure and fracture strains increased with higher contents of this waste, thereby increasing the absorbed energy of the concrete.
- The use of RCWTB also affected the deflection behavior under bending of the concrete specimens. First, it conditioned the compliance values, as this property was controlled at 7 days by the modulus of elasticity, and at 90 days the increased adhesion of the RCWTB fibers to the cementitious matrix limited that deformability. Second, percentage additions of up to 3.0 % reduced both the flexural strength and the failure deflection of the specimens, after which it increased, thus both properties demonstrated a close linear relationship regardless of age. Third, RCWTB provided load-bearing capacity from contents of 3.0 %, with the consequent increase in absorbed energy. The higher bond between RCWTB fibers and the cementitious matrix at advanced ages resulted in lower deflection at fracture and absorbed energy.
- Tensile deformability was conditioned by the splitting tensile strength, which remained approximately constant at percentage additions of up to 3.0 % RCWTB and decreased at higher contents. Furthermore, the addition of 6.0 % of this waste material provided a remarkable load-bearing capacity under the action of indirect-tensile stresses.

In global terms, the use of RCWTB increased the energy absorbed *per* unit of strength and *per* unit of carbon footprint. In addition, the longitudinal stress–strain behavior under compression and the pre-failure deflection performance under bending of the concrete specimens with percentage additions of RCWTB could be estimated with the results of the basic models corrected with adjustment coefficients, which is useful at the design stage. Therefore, the use of this waste from the wind-energy sector as an overall addition is an interesting and successful alternative that can increase the ductility and load-bearing capacity of concrete.

CRediT authorship contribution statement

Vanesa Ortega-López: Writing – original draft, Project administration, Investigation, Funding acquisition, Conceptualization. **Flora Faleschini:** Writing – review & editing, Supervision, Methodology, Data curation. **Nerea Hurtado-Alonso:** Methodology, Investigation, Formal analysis, Data curation. **Javier Manso-Morato:** Methodology, Investigation, Formal analysis, Data curation. **Víctor Revilla-Cuesta:** Writing – original draft, Software, Methodology, Investigation, Conceptualization.

Declaration of competing interest

The authors declare that they have no known competing financial interests or personal relationships that could have appeared to influence the work reported in this paper.

Data availability

As this is an experimental study, all the data generated are provided in the article through tables and graphs. The authors are pleased to provide any clarification.

Acknowledgements

This research work was supported by the Spanish Ministry of Universities within the framework of the State Program for the Promotion of Talent and its Employability in the R + D + i, State Mobility Subprogram of the State Plan for Scientific and Technical Research and Innovation 2021-2023 [CAS22/00013]; MICINN, AEI, EU, ERDF and NextGenerationEU/PRTR [grant numbers PID2020-113837RB-I00; PID2023-146642OB-I00; 10.13039/501100011033; TED2021-129715B-I00; FPU21/04364]; the Junta de Castilla y León (Regional Government) and ERDF [grant number UIC-231; BU033P23; BU066-22]; the University of Burgos [grant number SUCONS, Y135.GI]; and, finally, the University of Padova.

References

[1] Balagopal V, Panicker AS, Arathy MS, Sandeep S, Pillai SK. Influence of fibers on the mechanical properties of cementitious composites - a review. Mater Today Proc 2022;65:1846–50.
[2] Silva RV, De Brito J, Dhir RK. The influence of the use of recycled aggregates on the compressive strength of concrete: A review. Eur J Environ Civ Eng 2015;19(7):825–49.
[3] Liu Q, Cai L, Guo R. Experimental study on the mechanical behaviour of short chopped basalt fibre reinforced concrete beams. Structures 2022;45:1110–23.
[4] Shah YI, Hu Z, Du R. Stress evaluation of prestressed concrete beam based on cracking and incompatible deformation. J Civ Struct Health Monit 2022;12(6):1427–42.
[5] Toska K, Faleschini F, Zanini MA. Confinement of concrete with FRCM: Influence of bond aspects under cyclic axial loading. Constr Build Mater 2023;368:130432.
[6] Pacheco J, De Brito J, Chastre C, Evangelista L. Uncertainty Models of Reinforced Concrete Beams in Bending: Code Comparison and Recycled Aggregate Incorporation. J Struct Eng 2019;145(4):04019013.
[7] Revilla-Cuesta V, Skaf M, Santamaría A, Ortega-López V, Manso JM. Assessment of longitudinal and transversal plastic behavior of recycled aggregate self-compacting concrete: A two-way study. Constr Build Mater 2021;292:123426.
[8] Revilla-Cuesta V, Ortega-López V, Skaf M, Khan AUR, Manso JM. Deformational behavior of self-compacting concrete containing recycled aggregate, slag cement and green powders under compression and bending: Description and prediction adjustment. J Build Eng 2022;54:104611.
[9] Zhu H, Yu H, Ma H, Yang S. Uniaxial compressive stress-strain curves of magnesium oxysulfate cement concrete. Constr Build Mater 2020;232:117244.
[10] Dąbrowski M, Glinicki MA, Dziedzic K, Jóźwiak-Niedźwiedzka D, Sikorin S, Fateev VS, et al. Early age hardening of concrete with heavy aggregate in gamma radiation source – Impact on the modulus of elasticity and microstructural features. J Adv Concr Technol 2021;19(5):555–70.
[11] ACI-318-19. Building Code Requeriments for Structural Concrete. American Concrete Institute (ACI). 2019.
[12] EC-2. Eurocode 2: Design of concrete structures. Part 1-1: General rules and rules for buildings. CEN (European Committee for Standardization). 2010.
[13] Ortega-López V, García-Llona A, Revilla-Cuesta V, Santamaría A, San-José JT. Fiber-reinforcement and its effects on the mechanical properties of high-workability concretes manufactured with slag as aggregate and binder. J Build Eng 2021;43:102548.
[14] Yin P, Huang L, Yan L, Zhu D. Compressive behavior of concrete confined by CFRP and transverse spiral reinforcement. Part A: experimental study Mater Struct 2016;49(3):1001–11.
[15] Shayanfar J, Barros JAO, Rezazadeh M. Generalized Analysis-oriented model of FRP confined concrete circular columns. Compos Struct 2021;270:114026.
[16] Koziński K, Winnicki A. Experimental research and analysis of load capacity and deformability of slender high strength concrete columns in biaxial bending. Eng Struct 2016;107:47–65.
[17] Santamaría A, García-Llona A, Revilla-Cuesta V, Piñero I, Ortega-López V. Bending tests on building beams containing electric arc furnace slag and alternative binders and manufactured with energy-saving placement techniques. Structures 2021;32:1921–33.
[18] Bittner CM, Oettel V. Fiber reinforced concrete with natural plant fibers—investigations on the application of bamboo fibers in ultra-high performance concrete. Sustainability 2022;14(19):12011.
[19] Gouri Mohan L, Nazeer M, Nizad A, Suresh S. Fibre reinforced concrete - A state-of-the-art review. Intl J Earth Sci Eng. 2010;3(4 SPEC. ISSUE):634-42.
[20] Wu K, Zhang Y, Lin S, Liang Q, Qian S. Experimental study on mechanical properties of steel and steel fiber reinforced concrete beams. Struct Des Tall Spec Build 2022;31(17).
[21] Kan W, Yang Z, Yin W. Simulation of four-point bending fracture test of steel-fiber-reinforced concrete. Materials 2022;15(20):7146.
[22] Jayanth K, Prakash MNS, Suresh GS, Naveen BO. Studies on the behaviour of steel fibre-reinforced concrete under monotonic and repeated cyclic stress in compression. Arch Civ Mech Eng 2022;22(1):50.
[23] Ahmad J, Zhou Z. Mechanical properties of natural as well as synthetic fiber reinforced concrete: a review. Constr Build Mater 2022;333:127353.

[24] Dai JG, Huang BT, Shah SP. Recent advances in strain-hardening uhpc with synthetic fibers. J Compos Sci 2021;5(10):283.
[25] Liu C, Wang Y, Gao X, Zhang G, Liu H, Ma C, et al. Review of the strengthening methods and mechanical properties of recycled aggregate concrete (RAC). Crystals 2022;12(9):1321.
[26] Selvam M, Singh S. Material selection and mixture proportioning methods for sustainable roller-compacted concrete pavements. J Mater Civ Eng 2022;34(11).
[27] Ahmed HU, Faraj RH, Hilal N, Mohammed AA, Sherwani AFH. Use of recycled fibers in concrete composites: A systematic comprehensive review. Compos Part B: Eng 2021;215:108769.
[28] Awolusi TF, Oke OL, Atoyebi OD, Akinkurolere OO, Sojobi AO. Waste tires steel fiber in concrete: a review. Innov Infrastruct Solut 2021;6(1):34.
[29] Kilmartin-Lynch S, Saberian M, Li J, Roychand R, Zhang G. Preliminary evaluation of the feasibility of using polypropylene fibres from COVID-19 single-use face masks to improve the mechanical properties of concrete. J Clean Prod 2021;296:126460.
[30] WWEA. Statistics of the global wind-energy sector. World Wind Energy Association. 2022.
[31] Joustra J, Flipsen B, Balkenende R. Structural reuse of wind turbine blades through segmentation. Composite Part C Open Access 2021;5:100137.
[32] Rani M, Choudhary P, Krishnan V, Zafar S. A review on recycling and reuse methods for carbon fiber/glass fiber composites waste from wind turbine blades. Compos Part B: Eng 2021;215:108768.
[33] Fonte R, Xydis G. Wind turbine blade recycling: An evaluation of the European market potential for recycled composite materials. J Environ Manage 2021;287:112269.
[34] Pławecka K, Przybyła J, Korniejenko K, Lin WT, Cheng A, Łach M. Recycling of mechanically ground wind turbine blades as filler in geopolymer composite. Materials 2021;14(21):6539.
[35] Yazdanbakhsh A, Bank LC, Rieder KA, Tian Y, Chen C. Concrete with discrete slender elements from mechanically recycled wind turbine blades. Resour Conserv Recycl 2018;128:11–21.
[36] Baturkin D, Hisseine OA, Masmoudi R, Tagnit-Hamou A, Massicotte L. Valorization of recycled FRP materials from wind turbine blades in concrete. Resour Conserv Recycl 2021;174:105807.
[37] Xu GT, Liu MJ, Xiang Y, Fu B. Valorization of macro fibers recycled from decommissioned turbine blades as discrete reinforcement in concrete. J Clean Prod 2022;379:134550.
[38] Revilla-Cuesta V, Skaf M, Ortega-López V, Manso JM. Raw-crushed wind-turbine blade: Waste characterization and suitability for use in concrete production. Resour Conserv Recycl 2023;198:107160.
[39] EN-Euronorm. Rue de stassart, 36. Belgium-1050 Brussels, European Committee for Standardization.
[40] Konieczka R. Study of the cutting process during comminution of plastics. Kunstst Ger Plast 1989;79(7):25–6.
[41] Hamada HM, Al-Attar A, Shi J, Yahaya F, Al Jawahery MS, Yousif ST. Optimization of sustainable concrete characteristics incorporating palm oil clinker and nano-palm oil fuel ash using response surface methodology. Powder Technol 2023;413:118054.
[42] Revilla-Cuesta V, Manso-Morato J, Hurtado-Alonso N, Skaf M, Ortega-López V. Mechanical and environmental advantages of the revaluation of raw-crushed wind-turbine blades as a concrete component. J Build Eng 2024;82:108383.
[43] Alshahrani A, Kulasegaram S, Kundu A. Elastic modulus of self-compacting fibre reinforced concrete: Experimental approach and multi-scale simulation. Case Stud Constr Mater 2023;18:e01723.
[44] Islam MJ, Shahjalal M, Haque NMA. Mechanical and durability properties of concrete with recycled polypropylene waste plastic as a partial replacement of coarse aggregate. J Build Eng 2022;54:104597.
[45] Sosa ME, Villagrán Zaccardi YA, Zega CJ. A critical review of the resulting effective water-to-cement ratio of fine recycled aggregate concrete. Constr Build Mater 2021;313:125536.
[46] Al-Mansour A, Chen S, Xu C, Peng Y, Wang J, Ruan S, et al. Sustainable cement mortar with recycled plastics enabled by the matrix-aggregate compatibility improvement. Constr Build Mater 2022;318:125994.
[47] Abousnina R, Premasiri S, Anise V, Lokuge W, Vimonsatit V, Ferdous W, et al. Mechanical properties of macro polypropylene fibre-reinforced concrete. Polym 2021;13(23):4112.
[48] Arslan KM, Karagüler ME. Shrinkage cracking and mechanical properties of cementitious composites produced with multiwall carbon nano tubes and different types of polypropylene fibres. Constr Build Mater 2024;420:135599.
[49] Pratap Singh Rajawat S, Singh Rajput B, Jain G. Concrete strength analysis using waste plastic as a partial replacement for sand. Mater Today Proc 2022;62(P12):6824–31.
[50] Silva RV, De Brito J, Dhir RK. Establishing a relationship between modulus of elasticity and compressive strength of recycled aggregate concrete. J Clean Prod 2016;112:2171–86.
[51] CEB-FIP. Model Code Volumes 1 and 2. 2012.
[52] Salguero F, Romero S, Melgar SG, Prat F, Moreno F. Stress-strain curves of concrete under monotonic uniaxial compression: A systematic review. Inf Constr 2013;65(529):41–54.
[53] Dupen B. Applied Strength of Materials for engineering technology. 2016.
[54] Aghajanian A, Cimentada A, Behfarnia K, Brand AS, Thomas C. Microstructural analysis of siderurgical aggregate concrete reinforced with fibers. J Build Eng 2023;64:105543.
[55] Sahraei Moghadam A, Omidinasab F, Abdalikia M. The effect of initial strength of concrete wastes on the fresh and hardened properties of recycled concrete reinforced with recycled steel fibers. Constr Build Mater 2021;300:124284.
[56] Garcia-Llona A, Ortega-Lopez V, Piñero I, Santamaría A, Aguirre M. Effects of fiber material in concrete manufactured with electric arc furnace slag: Experimental and numerical study. Constr Build Mater 2022;316:125553.
[57] Hossain MU, Poon CS, Lo IMC, Cheng JCP. Comparative environmental evaluation of aggregate production from recycled waste materials and virgin sources by LCA. Resour Conserv Recycl 2016;109:67–77.
[58] Rebello TA, Zulcão R, Calmon JL, Gonçalves RF. Comparative life cycle assessment of ornamental stone processing waste recycling, sand, clay and limestone filler. Waste Manage Res 2019;37(2):186–95.
[59] Yang KH, Jung YB, Cho MS, Tae SH. Effect of supplementary cementitious materials on reduction of CO2 emissions from concrete. J Clean Prod 2015;103:774–83.